Development of novel anti-Kv 11.1 antibody-conjugated PEG-TiO2 nanoparticles for targeting pancreatic ductal adenocarcinoma cells

Angelica Sette, Jolanda Spadavecchia, Jessem Landoulsi, Sandra Casale, Bernard Haye, Olivia Crociani, Annarosa Arcangeli

HAL Id: hal-00983778

https://hal.sorbonne-universite.fr/hal-00983778v1

Submitted on 11 May 2015

RESEARCH PAPER

Development of novel anti-Kv 11.1 antibody-conjugated PEG–TiO$_2$ nanoparticles for targeting pancreatic ductal adenocarcinoma cells

Angelica Sette · Jolanda Spadavecchia · Jessem Landoulsi · Sandra Casale · Bernard Haye · Olivia Crociani · Annarosa Arcangeli

Abstract Titanium dioxide (TiO$_2$) has been widely used in many nanotechnology areas including nanomedicine, where it could be proposed for the photodynamic and sonodynamic cancer therapies. However, TiO$_2$ nanoformulations have been shown to be toxic for living cells. In this article, we report the development of a new delivery system, based on nontoxic TiO$_2$ nanoparticles, further conjugated with a monoclonal antibody against a novel and easily accessible tumor marker, e.g., the Kv 11.1 potassium channel. We synthesized, by simple solvothermal method, dicarboxylic acid-terminated PEG TiO$_2$ nanocrystals (PEG–TiO$_2$ NPs). Anti-Kv 11.1 monoclonal antibodies (Kv 11.1-Mab) were further linked to the terminal carboxylic acid groups. Proper conjugation was confirmed by X-ray photoelectron spectroscopy analysis. Kv 11.1-Mab-PEG–TiO$_2$ NPs efficiently recognized the specific Kv 11.1 antigen, both in vitro and in pancreatic ductal adenocarcinoma (PDAC) cells, which express the Kv 11.1 channel onto the plasma membrane. Both PEG TiO$_2$ and Kv 11.1-Mab-PEG–TiO$_2$ NPs were not cytotoxic, but only Kv 11.1-Mab-PEG–TiO$_2$ NPs were efficiently internalized into PDAC cells. Data gathered from this study may have further applications for the chemical design of nanostructures to be applied for therapeutic purposes in pancreatic cancer.

Keywords Nanoparticles · PEG–TiO$_2$ · XPS analysis · Kv 11.1 · Pancreatic cancer · Nanomedicine

Angelica Sette and Jolanda Spadavecchia have contributed equally to this work.

A. Sette · O. Crociani · A. Arcangeli (✉)
Section of Internal Medicine, Department of Experimental and Clinical Medicine, University of Florence, Viale GB Morgagni 50, 50134 Florence, Italy
e-mail: annarosa.arcangeli@unifi.it

J. Spadavecchia · J. Landoulsi · S. Casale
Laboratoire de Réactivité de Surface, UMR CNRS 7197, Université Pierre & Marie Curie-Paris VI, Site d'Ivry-Le Raphaël, 94200 Ivry-sur-Seine, France

B. Haye
Chimie de la Matière Condensée de Paris, Collège de France, Université Pierre & Marie Curie – Paris VI, 11 place Marcelin Berthelot, Paris, France

O. Crociani · A. Arcangeli
DI.V.A.L. Toscana srl, Via Madonna del Piano 6, 50019 Sesto Fiorentino (FI), Italy

Introduction

Nanophase engineering expands nowadays in rapidly growing number of structural and functional materials, both inorganic and organic. This allows the manipulation of nanostructures for different applications from mechanics to electronics (Caricato et al. 2007; Xu et al. 2011). Nanotechnology has recently received

great attention also for application in the biomedical field. In particular, nanoparticles (NPs) can be viewed as synthetic materials with considerable potential applications in biomedicine due to their unique ways to interact with matter (Wagner et al. 2006; Kim et al. 2010; Jokerst et al. 2011). NPs can be used either for diagnosis, as contrast agents in optical, photoacoustic, and magnetic resonance imaging, or for therapy. In the latter case, NPs can either be activated (e.g., by hyperthermia or photodynamic activation) or used as carriers for drug delivery. Nanocarriers are able to increase tumor exposure to therapeutic agents, improving treatment effects either by prolonging circulation times, protecting the carried drug from degradation, or enhancing tumor uptake (Fernandez-Fernandez et al. 2011).

Titanium dioxide (TiO_2) has been widely used in many nanotechnology areas such as paint industry, electronics, gas sensors, and environmental engineering (Song et al. 2008; De Marco et al. 2010). More recently, it has been applied to biomedicine. The production of reactive oxygen species (ROS) under ultraviolet and ultrasound irradiation (Ashikaga et al. 2000; Ninomiya 2012) makes TiO_2 an efficient photocatalyst. For these reasons, TiO_2 can be applied for the photodynamic and sonodynamic cancer therapies (Yamaguchi 2011). While TiO_2 is nontoxic (Fei Yin et al. 2013), the toxicity of nanoformulation of TiO_2 is debatable. This different behavior is related to the small size of NPs accompanied by a high specific surface area of interaction (Huang et al. 2010), as well as to their ability to easily cross biologic barriers such as the skin, lung, and intestine. Indeed, TiO_2 NPs were found to be toxic for mouse fibroblasts (Jin et al. 2008) and even more toxic for human cells (Lai et al. 2008). Consistently, human bronchial epithelial cells lost their viability at very low concentrations of TiO_2 NPs, an effect mediated by ROS production (Park et al. 2008). One strategy to prevent the toxicity of TiO_2 nanoformulations is their coating with polyethylene glycol (PEG). PEG is a hydrophilic, nonionic polymer that exhibits excellent biocompatibility (Jokerst et al. 2011). When used for drug delivery purposes, the addition of PEG to polymer particles produced an increased circulation time, which in turn prevented NPs uptake by the reticuloendothelial system (Jacobson et al. 2010).

Over the last few decades, the application of targeted therapeutic strategies to cancer has improved response and survival. To maximize the therapeutic activity while minimizing toxic side effects, it is possible to conjugate drugs to a targeted delivery system. Targeted NPs represent good drug delivery systems, to improve specific drug distribution and avoid systemic toxicity. Targeting of NPs can be achieved by either passive or active procedures. Passive targeting simply relies on NPs accumulation inside the tumor mass, an effect mediated by the so-called enhanced permeability and retention effect (Fernandez-Fernandez et al. 2011). However, low tumor specificity and suboptimal drug concentration at the tumor site strongly limit the efficacy of passive targeting approaches. For active targeting, it is necessary to incorporate, on the NPs surface, a targeting moiety (e.g., antibodies, peptides, etc.) able to bind an easily accessible and, hopefully, tumor-specific cell surface receptor. Such binding can facilitate NPs intracellular uptake and in turn, drug delivery. Preclinical studies showed that antibody-targeted NPs have better antitumor activity compared to nontargeted NPs, due to increased tumor localization (Zhang and Sun 2004; Kirpotin et al. 2006).

We report in this article, a new strategy for a targeted-therapeutic approach in cancer, based on actively targeted NPs. We synthesized dicarboxylic acid-terminated PEG TiO_2 nanocrystals by a simple one-step solvothermal method, and further conjugated the PEG–TiO_2 NPs with a monoclonal antibody (Arcangeli 2006), being able to bind a cell surface protein (e.g., the Kv 11.1 potassium channel), which is aberrantly expressed in many types of human cancers (D'Amico et al. 2013).

Materials and methods

Materials

Ti(IV) isopropoxide ($Ti(OPri)_4$ or TTIP 97 %; benzyl alcohol (BzOH ≥ 99 %)), (poly(ethyleneglycol) bis (carboxymethyl)ether) (PEG diacide MW:600), cysteamine (CYS), N-hydroxysuccinimide (NHS), 1-(3-dimethylaminopropyl)-N'-ethylcarbodiimide hydrochloride (EDC), DMF (dimethylformammide for molecule biology 99 %), buffer solution (PBS pH 7.4) were purchased from Sigma Aldrich (Saint-Quentin Fallavier, France). The S5-P peptide was synthesized by PRIMM company. All solvents were reagent grade and used without any further

purification. Experiments were carried out at room temperature if not specified otherwise.

TiO$_2$ synthesis and Kv 11.1-Mab immobilization

TiO$_2$ colloids were prepared according to the following procedure, as previously described by (Spadavecchia et al. 2011): in brief, 1 mL portion of TTIP (3.36 mmol) was added to 0.75 mL of PEG Diacide (MW: 600), along with 5 mL of BzOH (TTIP/PEG-diacid 1/5). The solution was stirred for 30 min at room temperature after which the reaction mixtures were transferred into a steel autoclave equipped with a Teflon cap and kept at 200 °C for 18 h. During this time, the solution turns from clear to yellow milky suspension. The reaction was then stopped, and the suspension was centrifuged two times (9,000 rpm for 30 min). The precipitate becomes white to slightly yellow upon washing with ethanol and dichloromethane two times and was dried under nitrogen. 10 mg of nPEG–TiO$_2$ was dissolved in 5 mL of DMF containing a solution of NHS (60 mM) and EDC (30 mM) in water for 4 h (activation). After rinsing in DMF and EtOH, the nPEG–TiO$_2$ was treated and centrifuged two times (9,000 rpm for 30 min). The precipitate becomes white to slightly yellow upon washing with ethanol two times and was dried under nitrogen. The binding of Kv 11.1-Mab was performed at pH 7.4 using PBS buffer solution. 50 µL (1 mg/mL) of Kv 11.1-Mab in PBS solution was added into 2 mL of PEG–TiO$_2$ NPs and stirred for 2 h at room temperature. After this time, Kv 11.1-Mab-PEG–TiO$_2$ nanoparticles were centrifuged two times (9,000 rpm for 30 min), dried under nitrogen, and analyzed by X-ray photoelectron spectroscopy (XPS) analysis (see below).

In order to check the specificity of the Kv 11.1-Mab-PEG–TiO$_2$, anti-IgG was also used and conjugated to PEG–TiO$_2$ following the same procedure used for the Kv 11.1-Mab antibody.

XPS analysis

XPS analyses were performed using a SPECS (Phoibos MCD 100), X-ray photoelectron spectrometer (SPECS, Germany) equipped with a monochromatized aluminum X-ray source ($hv = 1,486.74$ eV), and Phoibos 100 hemispherical energy analyzer. A pass energy of 20 eV was used for survey scan, and

10 eV as pass energy for narrow scans. The samples were fixed on the support, and no charge stabilization device was used. The pressure in the analysis chamber during measurement was around 10^{-10} Torr. The photoelectron collection angle (θ) between the normal to the sample surface and the analyzer axis was 0. The following sequence of spectra was recorded: survey spectrum, O 1s, N 1s, C 1s and Ti 2p. The data treatment was performed using the Casa XPS software (Casa Software Ltd., UK). The peaks were decomposed using a linear baseline, and a component shape defined by the product of a Gauss and Lorentz function, in 70:30 ratio. Molar concentration ratios were calculated using peak areas normalized according to Scofield factors.

ELISA assay

The ELISA assay was used to detect and verify the proper orientation of the Kv 11.1-Mab conjugated to PEG–TiO$_2$ nanoparticles. The S5-P peptide was used to cover a 96-well plate, and incubated overnight at 4 °C. After three washes with 0.05 %, Tween-20 in PBS, PEG–TiO$_2$, and Kv 11.1-Mab-PEG–TiO$_2$ NPs were diluted at different concentrations in BSA 3 % plus 0.05 % Tween-20 in PBS and incubated for 2 h at room temperature. 100 µL/well of antimouse secondary antibody (Sigma) (1:500) was dispensed and incubated for 1 h at room temperature. The assay was developed by the addition of 100 µL/well TMB substrate (Sigma), and the reaction was stopped with the addition of 100 µL/well of 0.5 M HCl. Plates were analyzed measuring the absorbance at 450 nm. For the ELISA assay on living cells, PANC-1 and NIH-3T3 were seeded to semiconfluence in 96-well plate in DMEM plus 10 % fetal bovine serum (FBS) and incubated overnight at 37 °C and 5 % CO$_2$. After three washes with PBS, Kv 11.1-Mab-PEG–TiO$_2$ and IgG-Mab-PEG–TiO$_2$ were diluted at different concentrations into culture medium and added to the cells for 2 h at room temperature. The following steps were the same as described above.

Measurement of cell viability

The viability of two pancreatic ductal adenocarcinoma (PDAC) cell lines, Panc-1 and MIA PaCa-2, in the presence of PEG–TiO$_2$ and Kv 11.1-Mab-PEG–TiO$_2$ NPs, was assessed using the WST-1 assay (Roche,

Mannheim, Germany). Cells were seeded into 96-well cell culture plates at a density of 3,000 cells/well in DMEM plus 10 % FBS. On the next day, cell medium was replaced by 100 μL of fresh medium containing PEG–TiO$_2$ or Kv 11.1-Mab-PEG–TiO$_2$ at different concentrations. Cells were cultured for 24 h in a humidified incubator at 37 °C and 5 % CO$_2$. Before the WST-1 assay, the medium in each sample was replaced with fresh medium that did not contain PEG–TiO$_2$. WST-1 reagent (10 μL) was added into each well, followed by incubation at 37 °C for 1 h. Then, the amount of formazan dye formed after WST-1 cleavage carried out by living cells was measured at 450 nm.

Immunofluorescence

MIAPaCa-2, Panc-1, and NIH-3T3 were plated onto glass coverslips coated with Fibronectin (Sigma) (20 μg/mL). The day after plating, coverslips were washed twice with PBS and fixed by treating for 1 h with 4 % paraformaldehyde in PBS, at room temperature. After three further washes in PBS, coverslips were incubated for 15 min in PBS plus 1 % SDS at room temperature for antigen retrieval, then treated for 15 min with 100 mM glycine at room temperature (to quench residual crosslinking activity of the formaldehyde) and permeabilized for 4 min with PBS plus 0.01 % Triton X-100. Unspecific binding sites were blocked for 30 min at room temperature with blocking solution (10 % fetal calf serum (FCS) in PBS) was then incubated for 1 h at room temperature with mouse anti-hERG1 monoclonal antibody (Enzo Life Technologies) (1 μg/mL) in blocking solution. After three washes with PBS, cells were incubated for 45 min at room temperature with Alexa-488-labeled secondary antimouse antibody (invitrogen) diluted in blocking solution (1:500). Coverslips were washed three times in PBS and mounted on glass microscope slides in fluorescence ProLong Gold Antifade Reagent with DAPI (invitrogen).

Transmission electron microscopy (TEM) analysis

TEM images of PEG–TiO$_2$ NPs were recorded using a JEOL JEM 1011 microscope operating at an accelerating voltage of 100 kV. The samples for TEM analyses were prepared by dropping a dilute solution of PEG–TiO$_2$ dissolved in dichloromethane onto carbon-coated copper grid and then allowing the solvent to evaporate.

TEM images of PDAC and NIH-3T3 cells treated with PEG–TiO$_2$ and Kv 11.1-Mab-PEG–TiO$_2$ NPs were acquired using the same apparatus, following the procedure described below. Panc-1 and MIA PaCa-2 cells were grown in a six-well plate, and then incubated with 0.01, 0.05, or 0.1 % of PEG–TiO$_2$ and with 0.01, 0.05, or 0.1 % of Kv 11.1-Mab-PEG–TiO$_2$ for 48 h in a humidified incubator at 37 °C and 5 % CO$_2$. Subsequently, cells were detached with 0.05 % trypsin plus 0.02 % EDTA, washed with PBS, and fixed in 2 % glutaraldehyde in phosphate buffer 0.1 M. Then, a procedure was applied, consisting of five steps: dehydration, impregnation, inclusion, ultramicrotomy, and contrasting.

Dehydration: the samples were gradually dehydrated by bath of ethanol 50, 70, and 95 % for 5 min each, and two baths of 10 min in ethanol 100 %. Then, ethanol was replaced by propylene oxide in two baths of 10 min: the first one in a mixing 50/50 ethanol propylene oxide, and the second in propylene oxide pure. Impregnation: the dehydrated samples were impregnated in a solution of Araldite (20 mL Araldite CY212; 22 mL DDSA—dodecenyl succinic anhydride, used as hardener; and 1.1 mL BDMA—benzyl dimethyl amine—used as accelerator). The impregnation has been done in three steps: the first one with a mixing of 2/3 volume of propylene oxide and 1/3 volume of araldite for 1 h, the second with a mixture of 1/3 volume of propylene oxide and 2/3 volume of araldite overnight at 4 °C and, finally, in pure Araldite. Inclusion: the samples impregnated by araldite were incubated at 60 °C for 3 days, to obtain hard blocks. Ultramicrotomy: blocks were cut in ultrathin section of 70 nm with an ultramicrotome (Ultracut Reichert, France). Contrasting: slides obtained were put onto copper grid and contrasted with a 50/50 mix of uranyl acetate 5 % and ethanol 100 % and rinsed with ethanol 50 %.

Results

Dicarboxylic acid-terminated PEG–TiO$_2$ nanocrystals were prepared according to the procedure previously described (Spadavecchia et al. 2011). In this procedure, PEG diacide plays twin activities: (i) as a relevant reagent precursor in the chemical synthesis,

Fig. 1 Schematic image of the formation of amide links between the COOH groups of the TiO$_2$ NP and NH$_2$ groups of the antibody

PEG-TiO$_2$NPs   Kv11.1-Mab   Kv11.1-Mab-PEG-TiO$_2$NPs
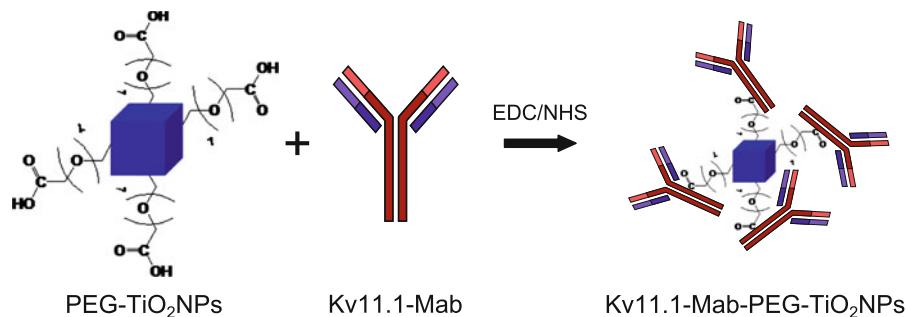
and (ii) as a stabilizer of the TiO$_2$ NP. In fact, the adsorbed PEG on the surface of TiO$_2$ particles enhances stabilization by both exerting steric effects and leading to the formation of a monodisperse phase.

The synthesized NPs were used as a support for peptide conjugation. We conjugated a monoclonal antibody directed against the Kv 11.1 potassium channel protein (Kv 11.1-Mab) which is over expressed in several types of human cancers (D'Amico et al. 2013). PEG–TiO$_2$ NPs were activated in EDC/NHS solution for 3 h, and then the antibody molecule was immobilized on the surface of activated NPs through the formation of amide links between the COOH groups of the TiO$_2$ NP and NH$_2$ groups of the antibody (Fig. 1).

The morphology of Kv 11.1-Mab-PEG–TiO$_2$ NPs, as revealed by TEM, showed separated and well-defined NPs with a unique cubic shape (Fig. 2b). Both the shape and size of Kv 11.1-Mab-PEG–TiO$_2$ NPs were identical to those of the PEG–TiO$_2$ NPs without peptide, as previously reported (Spadavecchia et al. 2011) (see also Fig. 2a). By analyzing several TEM images, Kv 11.1-Mab-PEG–TiO$_2$ NPs were observed to exhibit a narrow size distribution (near 7 nm, see the histogram in Fig. 2c). Moreover, from TEM pictures, it is possible to note that while PEG–TiO$_2$ NPs are close to each others, the distance between each Kv 11.1-Mab-PEG–TiO$_2$ NPs is greater by about 20 nm (compare pictures in Fig. 2a, b). Taking into account that the length of the Kv 11.1 Mab is about 15 nm (Foley et al. 2007), we can estimate that the antibody influence interparticle distance due a double combination of electrostatic and steric repulsion of the antibody linked to the PEG-chain present on the NPs. It is worth noting that all experiments were carried out at pH 7.4, a value at which the amino acids of the Kv 11.1-Mab (pI: 6.2–6.5) is positively charged. This implies that the intracellular uptake of Kv 11.1-Mab (see below) is favored only by the specific recognition

of the antibody to the Kv 11.1 protein expressed on the cancer cells. Finally, TEM images were also recorded on Kv 11.1-Mab-PEG–TiO$_2$NPs after incubation in FCS at 37 °C for 24 h: no relevant modification in terms of size and shape was observed (Fig. S1, Supplementary Section).

More direct evidence for the crystallinity of the NPs was confirmed by X-ray diffraction analysis (XRD) performed on Kv 11.1 Mab-PEG–TiO$_2$ NPs powder. Results showed particularly broad diffraction peaks, which are characteristic of very small crystallite sizes (Fig. 2d). The stability of the carboxylate ligand influences Ti–O–Ti bridge formation, thereby enhancing growth rates of various crystallographic planes. X-ray diffraction spectra also indicated the presence of NPs with a preferred growth orientation along the c-axis of the anatase lattice. As shown in Fig. 2d, all reflections correspond to anatase with a particle size of about 7 nm [calculated from the (101) reflection using Scherrer's equation, as previously performed (Ciccarella et al. 2009)]. These findings indicate the presence of NPs in anatase form, highly crystalline, and without apparent structural defects. Furthermore, the particle size determined by XRD is in a good agreement to that obtained by TEM.

The powders of Kv 11.1-Mab-PEG–TiO$_2$ NPs were also characterized by XPS analysis to check the nature of chemical functions present on the NP surface. Representative C 1s peaks recorded on TiO$_2$ NPs before and after the immobilization of the Kv 11.1-Mab are given in Fig. 3. The interpretation of this peak is based on the methodology developed specifically for biosystems (Rouxhet and Genet 2011) and other complex interfaces with biologic interest (Landoulsi et al. 2008; Spadavecchia et al. 2013). Before the immobilization of Kv 11.1 Mab, the C 1s peak exhibited (i) a component at 284.8 eV due to carbon bound only to carbon and/or hydrogen [C–(C,H)]; (ii)
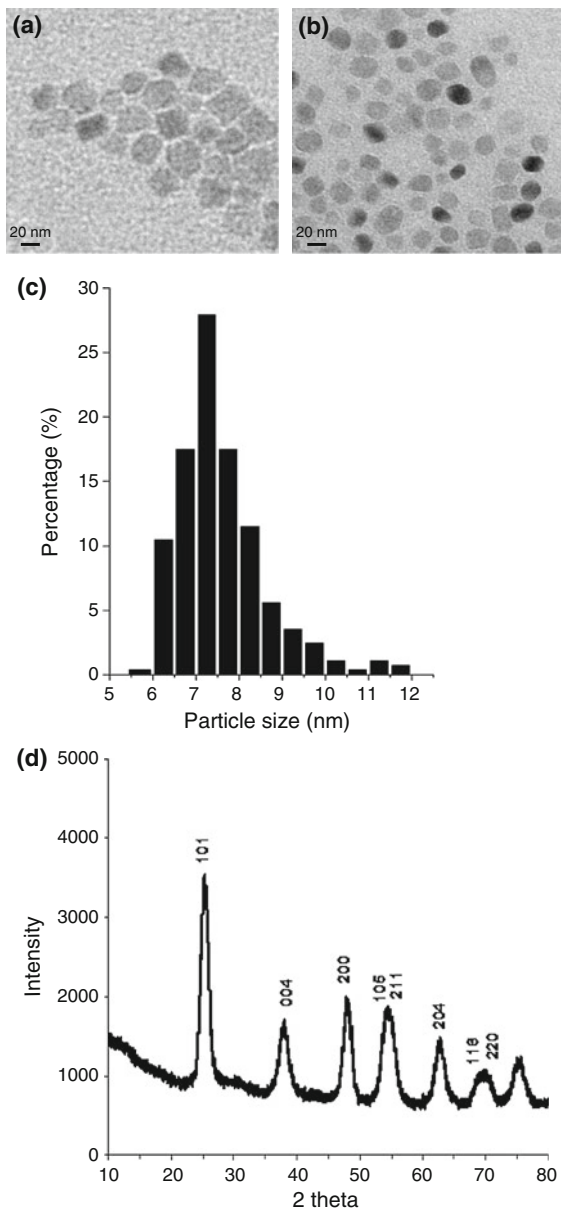
Fig. 2 Structural analysis of Kv 11.1-Mab-PEG–TiO$_2$: **a** TEM pictures of clusters of PEG–TiO$_2$ NPs in solution; **b** TEM pictures of clusters of Kv 11.1-Mab-PEG–TiO$_2$ NPs in solution; **c** particle size distribution of Kv 11.1-Mab-PEG–TiO$_2$ NPs; and **d** XRD Pattern

Fig. 3 XPS analysis. C 1s and N 1s peaks recorded on PEG–TiO$_2$ NPs **a** before and **b** after immobilization of Kv 11.1-Mab

an intense component at about 286.3 eV due to carbon making a single bond with oxygen and/or nitrogen [C–(O,N)], which reveals the dominating presence of PEG function; and (iii) a component at about 289.0 eV attributed to carboxyl and ester functions [O–C=O]. 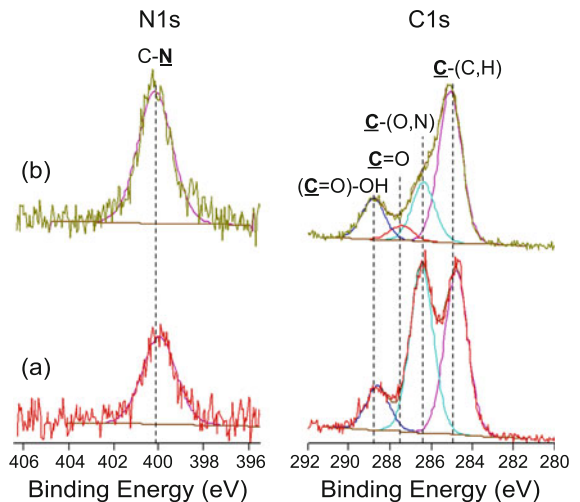These results confirm the expectations regarding the chemical function present on the nPEG–TiO$_2$ NPs. After immobilization of the Kv 11.1-Mab, a significant decrease of the contribution at 286.3 eV is observed, and a contribution at about 287.9 eV, due to carbon making one double bond [C=O] with oxygen in amide, appeared. This suggests that the protein is present on the NP surface. Further support to these findings is given by the analysis of the N 1s peak (Fig. 3), which shows a noticeable increase after protein immobilization. The main component in the N 1s peak is situated at about 400.0 eV, attributable to amide or amine [C–N], with no additional components near 401.6 eV, due to protonated amine. The presence of nitrogen before the immobilization of the Kv 11.1-Mab is due to compounds from adventitious contamination, as broadly observed with XPS on high energy solid surfaces.

In order to achieve a NP system that is capable of targeting specific cells, the binding procedure must preserve the biologic activity, and in particular, the specificity, of the antibody. Therefore, we first evaluated the binding capacity and specificity of the Kv 11.1-Mab-PEG–TiO$_2$NPs, performing an ELISA assay against the peptide (S5-P peptide) used for raising the antibody (Guasti et al. 2008). This assay can be also used to verify the proper orientation of the Kv 11.1-Mab conjugated to the PEG–TiO$_2$ NPs. Figure 4a shows the 450-nm absorbance values obtained after incubation of either PEG–TiO$_2$ or Kv 11.1-Mab-PEG–TiO$_2$ NPs onto S5-P peptide-coated
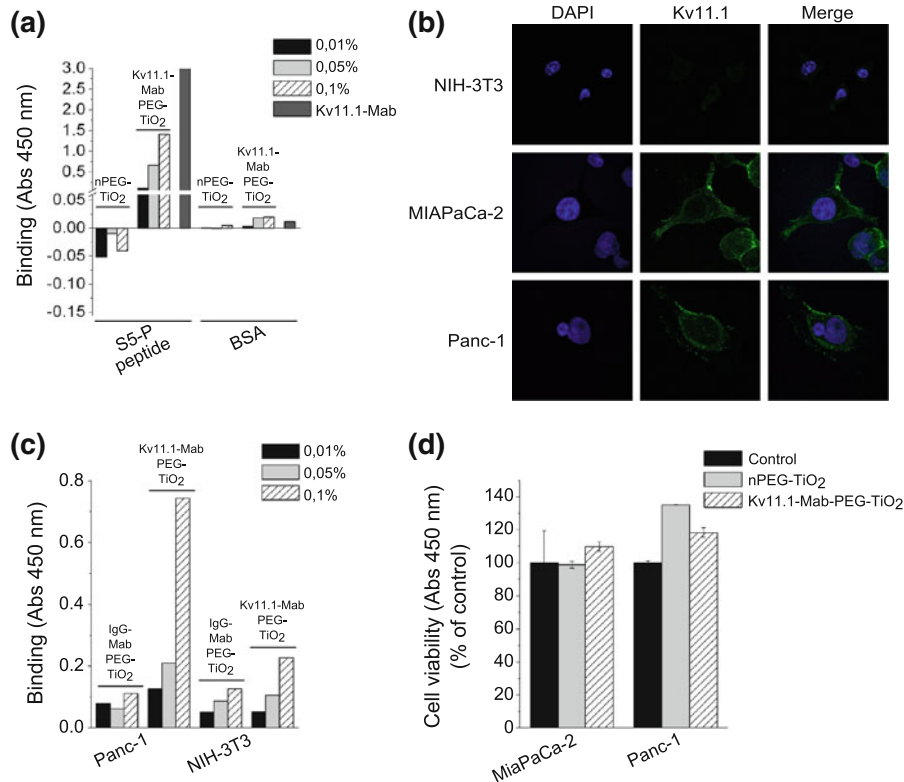
Fig. 4 NPs' interaction with PDAC cells: **a** binding specificity of Kv 11.1-Mab-PEG–TiO$_2$ NPs determined through an ELISA assay performed on the S5P peptide; **b** Kv 11.1 expression in NIH-3T3, MIAPaCa-2, and Panc-1 cells. Immunofluorescence was performed on cells seeded onto glass slides coated with 20 μg/mL Fibronectin, by means of Kv 11.1-Mab and Alexa-488-conjugated secondary antibody. Photographs were taken using a C1 confocal microscope (Nikon); **c** binding of Kv 11.1-Mab-PEG–TiO$_2$ NPs on cells: MIAPaCa-2 and NIH-3T3 cells were treated with different concentrations of Kv 11.1-Mab-PEG–TiO$_2$ and IgG-Mab-PEG–TiO$_2$; **d** cell viability (WST-1) assay performed on MIAPaCa-2 and Panc-1 cells in the presence of either PEG–TiO$_2$ or Kv 11.1-Mab-PEG–TiO$_2$ NPs, both at 0.1 % concentration

or BSA-coated wells. PEG–TiO$_2$ NPs showed no binding to the S5-P peptide, whereas Kv 11.1-Mab-PEG–TiO$_2$ NPs recognized and bound the S5-P peptide-coated wells in a dose-dependent manner. In particular, Kv 11.1-Mab-PEG–TiO$_2$ NPs at 0.1 % concentration gave an absorbance value of roughly half of that obtained with 10 μg/mL of the whole antibody molecule, suggesting good binding efficiency of the antibody to the NPs, as well as the maintenance of good antigen recognition. Conversely, no binding of Kv 11.1-Mab-PEG–TiO$_2$ NPs to BSA-coated wells was detected. We can conclude that the Kv 11.1-Mab, also when bound to PEG–TiO$_2$ NPs, efficiently and specifically binds its proper antigen.

We then assessed whether Kv 11.1-Mab-PEG–TiO$_2$ NPs properly recognized the whole antigen, e.g., the Kv 11.1 potassium channel, when expressed on the plasma membrane of living cells. To this purpose, we used two human PDAC cell lines (MIAPaCa-2 and Panc-1), which express Kv 11.1 at the plasma membrane level (see immunofluorescence pictures in Fig. 4b). On the other hand, NIH-3T3 cells, which are devoid of Kv 11.1 expression (Fig. 4b) were used as negative control. Figure 4c shows data relative to Panc-1 and NIH-3T3 cells: Kv 11.1-Mab-PEG–TiO$_2$ NPs efficiently bound Panc-1 cells, in a dose-dependent manner, whereas they did not bind NIH-3T3 cells. On the other hand, NPs conjugated with an irrelevant antibody (IgG-Mab-PEG–TiO$_2$) did not bind either Panc-1 or NIH-3T3 cells. Hence, Kv 11.1-Mab-PEG–TiO$_2$ NPs efficiently and specifically bind their antigen, when it is physiologically expressed onto the plasma membrane of tumor cells.

We then assessed the cytotoxicity of PEG–TiO$_2$ and Kv 11.1-Mab-PEG–TiO$_2$ NPs, both diluted at 0.1 % concentration into culture medium, through the

Fig. 5 TEM pictures of PDAC cells trated with PEG–TiO$_2$ NPs or Kv 11.1-Mab–PEG–TiO$_2$ NPs: **a**, **c** Panc-1 treated with PEG–TiO$_2$ NPs (0.1 %). **b** MIAPaCa-2 treated with Kv 11.1-Mab-PEG–TiO$_2$ NPs (0.1 %); **d** Panc-1 treated with Kv 11.1-Mab-PEG–TiO$_2$ NPs (0.1 %); TEM was performed after exposure for 48 h to either PEG–TiO$_2$ or Kv 11.1-Mab-PEG–TiO$_2$ NPs. *Scale bars* are reported on the *bottom left* of each panel

nPEG-TiO$_2$ Kv11.1-PEG-TiO$_2$
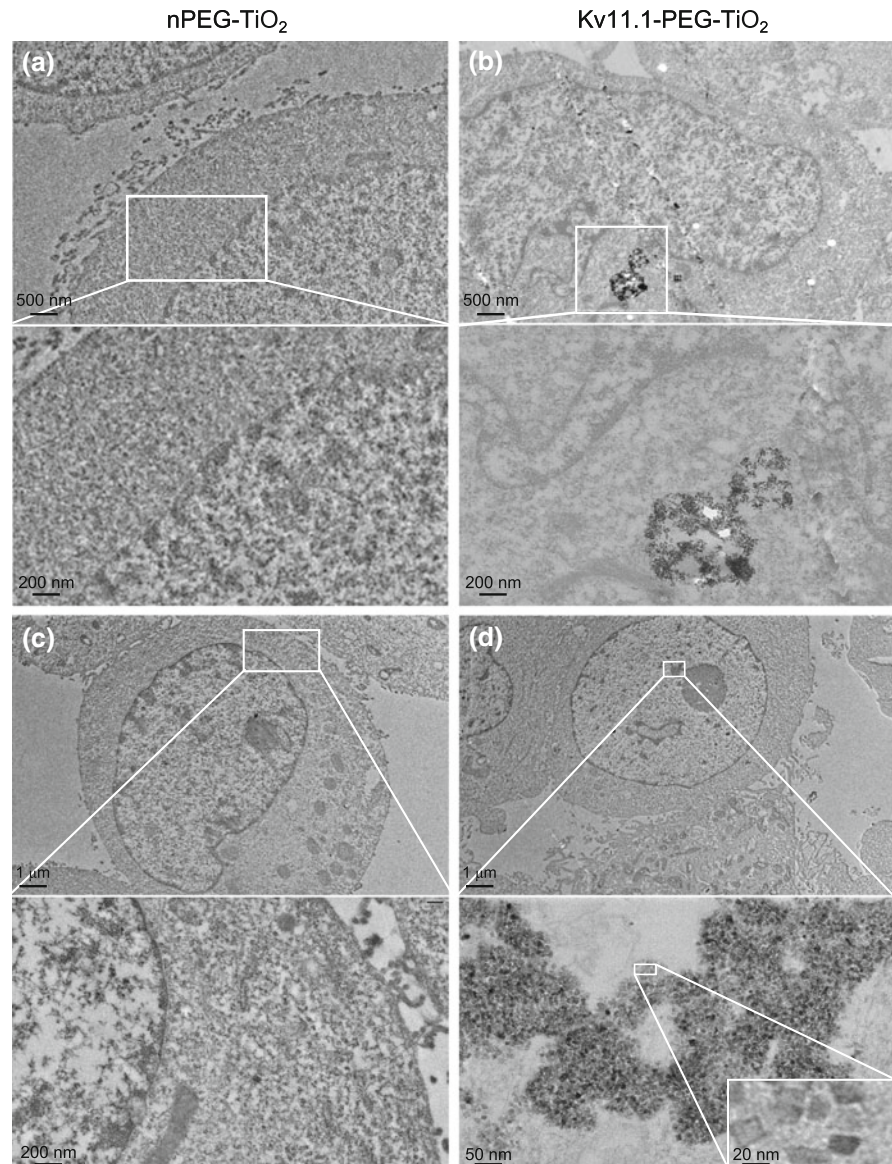
WST1 assay. Both MiaPaCa-2 and Panc-1 cells were analyzed, and the corresponding results are shown in Fig. 4d: neither PEG–TiO$_2$ nor Kv 11.1-Mab-PEG–TiO$_2$ NPs affected cell viability, in both types of cells.

Finally, we evaluated by TEM analysis whether Kv 11.1-Mab-PEG–TiO$_2$ NPs could by internalized into PDAC cells. TEM was performed on 70-nm sections of either MIAPaCa-2 or PANC-1 cells, after exposure for 48 h to either PEG–TiO$_2$ or Kv 11.1-Mab-PEG–TiO$_2$ NPs, both at 0.1 % concentration. Pictures are shown in Fig. 5 and in the Supplementary Section, Fig. S2. Kv 11.1-MAb-PEG–TiO$_2$ NPs were found to

be well internalized (see Fig. 5b), whereas PEG–TiO$_2$ NPs showed undetectable intracellular localization (Fig. 5a, c). Both panels (a) and (b) show noncontrasted cells, and the NPs are clearly evident (see the white box in panel (b) and its higher magnification below). Only Kv 11.1-Mab-TiO$_2$ NPs are present inside the cell, as evidenced in the picture in panel (b). In particular, a large endocytotic vesicle is present inside the cytoplasm, filled with clusters of NPs. In some cells, we found that Kv 11.1-MAb-PEG–TiO$_2$ NPs reached the nucleus (Fig. 5d, S2). Note that panels (c) and (d) show contrasted cells, and the NPs

are hence more conspicuous only in the magnifications reported below the corresponding panels. The size and shape of the Kv 11.1-MAb-PEG–TiO$_2$ NPs internalized into the cells remained unchanged compared with NPs in aqueous solution (compare the magnification with the scale bar at 20 nm in the inset to Figs. 2b, 5d).

Discussion

TiO$_2$ nanoformulations have been widely used in many nanotechnology areas, but their use in nanomedicine for drug delivery purposes is still hampered by the high toxicity that TiO$_2$ NPs exert on living cells. In this article, we report the development of new, nontoxic TiO$_2$ nanoparticles, further conjugated with a monoclonal antibody against a novel and easily accessible tumor marker, e.g., the Kv 11.1 potassium channel, proposed for drug delivery purposes.

We synthesized, by simple solvothermal method, dicarboxylic acid-terminated PEG–TiO$_2$ NPs, further conjugated with the Kv 11.1-Mab, characterized by a high homogenous shape and extremely small size (about 7 nm). Hence, we obtained TiO$_2$ NPs with a large surface area, and therefore with an ensuing increase of the number of available surface-active sizes (Di Paola et al. 2008). The narrow-size distribution should lead to a high photonic efficiency favoring a higher interfacial charge carrier transfer rate and a better photocatalytic activity of NPs.

PEG–TiO$_2$ NPs were further conjugated with a monoclonal antibody directed against a novel tumor target, e.g., Kv 11.1 potassium channel. While the relevance of ion channels in tumor cell biology has been increasing in the recent years (Arcangeli and Yuan 2011) this is the first article exploiting voltage-dependent potassium channels as targets for nanodelivery. Only a recent article (Li et al. 2013) showed the development of nanoparticles carrying small interfering RNAs against Kv 11.1 channels, further stressing the relevance of these channel proteins in innovative cancer treatments. We showed that Kv 11.1-Mab-PEG–TiO$_2$ NPs efficiently and specifically recognized the specific Kv 11.1 antigen, both in vitro and in PDAC cells which express the Kv 11.1 channel onto the plasma membrane. The proper orientation of the targeting moiety promotes the antigen binding and the subsequent spontaneous internalization by the target cells without using physical methods such as electroporation (Xu et al. 2007). Indeed, we proved this fact by showing that only Kv 11.1-MAb-PEG–TiO$_2$ NPs are well internalized into PDAC cells. In particular, we observed large endocytotic vesicle inside the cytoplasm, filled with clusters of NPs. Such appearance is consistent with a mechanism of endocytosis underlying Kv 11.1-MAb-PEG–TiO$_2$ NPs intracellular uptake, similar to that reported for other NPs in other cellular types (Wilhelm et al. 2003; Riviere et al. 2007). It is worth noting that the uptake kinetics of NPs by cells have been only slightly characterized and quantified as a function of their size and shape (Chithrani et al. 2006). Most studies have focused on liposomes (Chenevier et al. 2000) and polymer particles (Jaulin et al. 2000; Alyaudtin et al. 2001) which are generally larger than 100 nm (Alyaudtin et al. 2001).Very recently (Grudzinski et al. 2013), carbon-coated iron NPs were shown to be internalized into melanoma cells, with a pattern of internalization similar to that observed by us.

Finally, we showed that both PEG TiO$_2$ and Kv 11.1-Mab-PEG–TiO$_2$ NPs were not cytotoxic to PDAC cells. Since other studies have shown a significant toxicity of TiO$_2$ NPs (Jin et al. 2008; Okuda-Shimazaki et al. 2010), our data stress the prominent role of the coating (e.g., PEG) in avoiding cytotoxicity (Mano et al. 2012), a fact that could be related to either the nature or the charge of the coating.

The lack of cytotoxicity stresses even more the possible applications of the targeted NPs, which we have developed for cancer therapy. In fact, our NPs could be used for therapeutical purposes by either exploiting the photocatalytic features of TiO$_2$ with the ensuing ROS production or introducing new moieties (e.g., porphyrins, phthalocyanines) or cytotoxic drugs inside the NPs. Due to the low toxicity of the PEG–TiO$_2$ NPs that we have developed, both these approaches will be tested in vivo using appropriate PDAC mouse models.

References

Alyaudtin RN, Reichel A, Lobenberg R, Ramge P, Kreuter J, Begley DJ (2001) Interaction of poly(butylcyanoacrylate) nanoparticles with the blood-brain barrier in vivo and in vitro. J Drug Target 9(3):209–221

Arcangeli A, Crociani O (2006). Patent FI20,06A,000,008

Arcangeli A, Yuan JX (2011) American Journal of Physiology-Cell Physiology theme: ion channels and transporters in cancer. Am J Physiol Cell Physiol 301(2):C253–254

Ashikaga T, Wada M, Kobayashi H, Mori M, Katsumura Y, Fukui H, Kato S, Yamaguchi M, Takamatsu T (2000) Effect of the photocatalytic activity of TiO$_2$ on plasmid DNA. Mutat Res 466:1–7

Caricato AP, Capone S, Ciccarella G, Martino M, Rella R, Romano F, Spadavecchia J, Taurino A, Tunno T, Valerini D (2007) TiO$_2$ nanoparticle thin film deposition by matrix assisted pulsed laser evaporation for sensing applications. Appl Surf Sci 253(19):7937–7941

Chenevier P, Veyret B, Roux D, Henry-Toulme N (2000) Interaction of cationic colloids at the surface of J774 cells: a kinetic analysis. Biophys J 79:1298–1309

Chithrani BD, Ghazani AA, Chan WC (2006) Determining the size and shape dependence of gold nanoparticle uptake into mammalian cells. Nano Lett 6(4):662–668

Ciccarella G, Cingolani R, De Marco L, Gigli G, Melcarne G., Martina F, Matteucci F, Spadavecchia J (2009). World Patent 2009/101640A1

D'Amico M, Gasparoli L, Arcangeli A (2013) Potassium channels: novel emerging biomarkers and targets for therapy in cancer. Recent Pat Anticancer Drug Discov 8:53–65

De Marco L, Manca M, Giannuzzi R, Malara F, Melcarne G, Ciccarella G, Zama I, Cingolani R, Gigli G (2010) Novel preparation method of TiO$_2$-nanorod-based photoelectrodes for dye-sensitized solar cells with improved light-harvesting efficiency. J Phys Chem C 114(9):4228–4236

Di Paola A, Cufalo G, Addamo M, Bellardita M, Campostrini R, Ischia M, Ceccato R, Palmisano L (2008) Photocatalytic activity of nanocrystalline TiO$_2$ (brookite, rutile and brookite-based) powders prepared by thermohydrolysis of TiCl$_4$ in aqueous chloride solutions. Colloids Surf A 317(1–3):366–376

Fernandez-Fernandez A, Manchanda R, McGoron AJ (2011) Theranostic applications of nanomaterials in cancer: drug delivery, image-guided. Appl Biochem Biotechnol 165(7–8):1628–1651

Foley JO, Nelson KE, Mashadi-Hossein A, Finlayson BA, Yager P (2007) Concentration gradient immunoassay. 2. Computational modeling for analysis and optimization. Anal Chem 79(10):3549–3553

Grudzinski IP, Bystrzejewski M, Cywinska MA, Kosmider A, Poplawska M, Cieszanowski A, Ostrowska A (2013) Cytotoxicity evaluation of carbon-encapsulated iron nanoparticles in melanoma cells and dermal fibroblasts. J Nanopart Res 15:1835

Guasti L, Crociani O, Redaelli E, Pillozzi S, Polvani S, Masselli M, Mello T, Galli A, Amedei A, Wymore RS, Wanke E, Arcangeli A (2008) Identification of a posttranslational mechanism for the regulation of hERG1K+channel

expression and hERG1 current density in tumor cells. Mol Cell Biol 28:5043–5060

Huang CC, Aronstam RS, Chen DR, Huang YW (2010) Oxidative stress, calcium homeostasis, and altered gene expression in human lung epithelial cells exposed to ZnO nanoparticles. Toxicol In Vitro 24:45–55

Jacobson GB, Gonzalez-Gonzalez E, Spitler R, Shinde R, Leake D, Kaspar RL, Contag CH, Zare RN (2010) Biodegradable nanoparticles with sustained release of functional siRNA in skin. J Pharm Sci 99(10):4261–4266

Jaulin N, Appel M, Passirani C, Barratt G, Labarre D (2000) Reduction of the uptake by a macrophagic cell line of nanoparticles bearing heparin or dextran covalently bound to poly(methyl methacrylate). J Drug Target 8:165–172

Jin CY, Zhu BS, Wang XF, Lu QH (2008) Cytotoxicity of titanium dioxide nanoparticles in mouse fibroblast cells. Chem Res Toxicol 21(9):1871–1877

Jokerst JV, Lobovkina T, Zare RN, Gambhir SS (2011) Nanoparticle PEGylation for imaging and therapy. Nanomedicine (Lond) 6(4):715–728

Kim BY, Rutka JT, Chan WC (2010) Nanomedicine. N Engl J Med 363(25):2434–2443

Kirpotin DB, Drummond DC, Shao Y, Shalaby MR, Hong K, Nielsen UB, Marks JD, Benz CC, Park JW (2006) Antibody targeting of long-circulating lipidic nanoparticles does not increase. Cancer Res 66(13):6732–6740

Lai JC, Lai MB, Jandhyam S, Dukhande VV, Bhushan A, Daniels CK, Leung SW (2008) Exposure to titanium dioxide and other metallic oxide nanoparticles induces cytotoxicity on human neural cells and fibroblasts. Int J Nanomedicine 3(4):533–545

Landoulsi J, Genet MJ, Richard C, El Kirat K, Pulvin S, Rouxhet PG (2008) Evolution of the passive film and organic constituents at the surface of stainless steel immersed in fresh water. J Colloid Interface Sci 318:278–289

Li G, Hu Z, Yin H, Zhang Y, Huang X, Wang S, Li W (2013) A novel dendritic nanocarrier of polyamidoamine-polyethylene glycol-cyclic RGD for "smart" small interfering RNA delivery and in vitro antitumor effects by human ether-a-go–go-related gene silencing in anaplastic thyroid carcinoma cells. Int J Nanomedicine 8:1293–1306

Mano SS, Kanehira K, Sonezaki S, Taniguchi A (2012) Effect of polyethylene glycol modification of TiO$_2$ nanoparticles on cytotoxicity and gene expressions in human cell lines. Int J Mol Sci 13:3703–3717

Ninomiya K, Ogino C, Shema S, Sonoke S, Kuroda S, Shimizu N (2012) Targeted sonodynamic therapy using protein-modified TiO$_2$ nanoparticles. Ultrason Sonochem 19:607–614

Okuda-Shimazaki J, Takaku S, Kanehira K, Sonezaki S, Taniguchi A (2010) Effects of titanium dioxide nanoparticle aggregate size on gene expression. Int J Mol Sci 11(6):2383–2392

Park EJ, Yi J, Chung KH, Ryu DY, Choi J, Park K (2008) Oxidative stress and apoptosis induced by titanium dioxide nanoparticles in cultured BEAS-2B cells. Toxicol Lett 180:222–229

Riviere C, Wilhelm C, Cousin F, Dupuis V, Gazeau F, Perzynski R (2007) Internal structure of magnetic endosomes. Eur Phys J E 22(1):1–10

Rouxhet PG, Genet MJ (2011) XPS analysis of bio-organic systems. Surf Interface Anal 43(12):1453–1470

Song M, Pan C, Li J, Zhang R, Wang X, Gu Z (2008) Blends of TiO_2 nanoparticles and poly (N-isopropylacrylamide)-co-polystyrene nanofibers as a means to promote the biorecognition of an anticancer drug. Talanta 75:1035–1040

Spadavecchia J, Boujday S, Landoulsi J, Pradier CM (2011) nPEG-TiO_2 nanoparticles: a facile route to elaborate nanostructured surfaces for biological applications. ACS Appl Mater Interfaces 3(7):2637–2642

Spadavecchia J, Methivier C, Landoulsi J, Pradier CM (2013) Interaction of Zn(II) porphyrin with TiO_2 nanoparticles: from mechanism to synthesis of hybrid nanomaterials. ChemPhysChem 14(11):2462–2469

Wagner V, Dullaart A, Bock AK, Zweck A (2006) The emerging nanomedicine landscape. Nat Biotechnol 24(10):1211–1217

Wilhelm C, Billotey C, Roger J, Pons JN, Bacri JC, Gazeau F (2003) Intracellular uptake of anionic superparamagnetic nanoparticles as a function of their surface coating. Biomaterials 24:1001–1011

Xu J, Sun Y, Huang J, Chen C, Liu G, Jiang Y, Zhao Y, Jiang Z (2007) Photokilling cancer cells using highly cell-specific antibody-TiO_2 bioconjugates and electroporation. Bioelectrochemistry 71:217–222

Xu M, Gao Y, Moreno EM, Kunst M, Muhler M, Wang Y, Idriss H, Wöll C (2011) Photocatalytic activity of bulk TiO_2 anatase and rutile single crystals using infrared absorption spectroscopy. Phys Rev Lett 106(13):138302

Yamaguchi S, Kobayashi H, Narita T, Kanehira K, Sonezaki S, Kudo N, Kubota Y, Terasaka S, Houkin K (2011) Sonodynamic therapy using water-dispersed TiO_2-polyethylene glycol compound on glioma cells: comparison of cytotoxic mechanism with photodynamic therapy. Ultrason Sonochem 18:1197–1204

Yin ZF, Wu L, Yang HG, Su YH (2013) Recent progress in biomedical applications of titanium dioxide. Phys Chem Chem Phys 15(14):4844–4858

Zhang AP, Sun YP (2004) Photocatalytic killing effect of TiO_2 nanoparticles on Ls-174-t human colon carcinoma cells. World J Gastroenterol 10(21):3191–3193